

Elastic analysis in 3D anisotropic functionally graded solids by the MLPG

J. Sladek¹, V. Sladek¹ and P. Sulek²

Abstract: A meshless method based on the local Petrov-Galerkin approach is proposed for solution of static and elastodynamic problems in 3-D continuously non-homogeneous anisotropic bodies. Functionally graded materials (FGM) are multi-phase materials with the phase volume fractions varying gradually in space, in a pre-determined profile. The Heaviside step function is used as the test functions in the local weak form resulting into the derived local integral equations (LIEs). For transient elastodynamic problems either the Laplace transform or the time difference techniques are applied. Nodal points are randomly distributed in the 3D analyzed domain and each node is surrounded by a spherical subdomain to which a local integral equation is applied. The final form of the local integral equations has a pure contour character only in elastostatics. In elastodynamics an additional domain integral is involved due to inertia terms. The spatial variation of the displacement is approximated by the moving least-square (MLS) scheme.

Keywords: meshless method, local weak form, Heaviside step function, moving least squares interpolation, Laplace transform, Houbolt method

1 Introduction

Functionally graded materials are multi-phase materials with the phase volume fractions varying gradually in space, in a pre-determined profile. This results in continuously graded thermo-mechanical properties at the (macroscopic) structural scale. Often, these spatial gradients in material behaviour render FGMs as superior to conventional composites. FGMs possess some advantages over conventional composites because of their continuously graded structures and properties [Suresh and Mortensen (1998); Miyamoto et al. (1999)]. FGMs may exhibit isotropic or anisotropic material properties, depending on the processing technique and the

¹ Institute of Construction and Architecture, Slovak Academy of Sciences, 84503 Bratislava, Slovakia

² Department of Mechanics, Slovak Technical University, 81243 Bratislava, Slovakia

practical engineering requirements. Recent progress in the development and research of FGMs has also enhanced interests in the development of numerical methods for the solution of elastic and elastodynamic problems in continuously non-homogeneous solids. The first numerical studies of FGMs have been carried out using the Finite Element Method [Santare and Lambros (2000); Anlas et al. (2000); Kim and Paulino (2002)]. The boundary element method (BEM) is very powerful computational method if the fundamental solution is available. The anisotropy increases the number of elastic constants in Hooke's law, hence the construction of fundamental solutions become difficult even in a homogeneous medium. The fundamental solution is available in a closed form for 2D problems in a homogeneous anisotropic solid [Eshelby et al. (1953); Schlar (1994)] and it is given in a complex variable space. Several numerical analyses have been applied to 2-d elastostatic problems [Cruse and Swedlow (1971); Brebbia et al. (1984)] and in specific problems like half-plane [Dumir and Mehta (1987); Pan et al. (1998)], fracture mechanics [Snyder and Cruse (1975); Clements and Haselgrove (1983); Sollero and Aliabadi (1993); Pan and Amadei (1996); Ang and Telles (2004)] and piezoelectric solids [Pan (1999)]. Closed form fundamental solutions for 3D anisotropic elasticity exist for special cases like transversally isotropic or cubic homogeneous media [Ding et al. (1997)]. Recently, Shiah et al. (2008) have derived the explicit form of the fundamental solutions for displacements and stresses in 3D anisotropic elastic solids.

Governing equations for continuously nonhomogeneous solids are more complicated than for a homogeneous counterpart. Therefore, fundamental solutions for general functionally graded materials are not available in 2D and 3D elasticity. Recently, fundamental solutions for 2D and 3D elastic problems in exponentially graded isotropic materials have been derived [Martin et al. (2002); Chan et al. (2004); Criado et al. (2008)]. It was leading to develop the Boundary Element Method for a special class of functionally graded materials in 3-D elasticity [Criado et al. (2007)].

In spite of the great success of the finite and boundary element methods as effective numerical tools for the solution of boundary value problems on complex domains, there is still a growing interest in development of new advanced methods. Many meshless formulations are becoming to be popular due to their high adaptivity and a low cost to prepare input data for numerical analysis. A variety of meshless methods has been proposed so far [Belytschko et al. (1996); Atluri and Zhu (1998); Zhu et al. (1998); Atluri (2004)]. Many of them are derived from a weak-form formulation on global domain [Belytschko et al. (1994)] or a set of local subdomains [Zhu et al. (1998); Atluri and Shen (2002); Atluri et al. (2003); Sladek et al. (2003a,b); Mikhailov (2002)]. In the global formulation background cells are required for the

integration of the weak form. In methods based on local weak-form formulation no cells are required and therefore they are often referred to call as truly meshless methods. If for the geometry of subdomains a simple form is chosen, numerical integrations can be easily carried out over them. The meshless local Petrov-Galerkin (MLPG) method is fundamental base for the derivation of many meshless formulations, since trial and test functions are chosen from different functional spaces. The fundamental solution as the test function is leading to accurate numerical results and it was utilized in former papers for isotropic homogeneous and continuously nonhomogeneous bodies under static [Atluri et al. (2000); Sladek et al. (2000)], dynamic loads [Sladek et al. (2003a, b)] and thermoelasticity [Sladek et al. (2001)]. However, in an anisotropic elasticity the fundamental solution is complex or unavailable in a closed form. From complex fundamental solution it is very difficult to derive the Green's function which vanishes on the local boundary of circular subdomain. It is inappropriate to utilize such a non-vanishing fundamental solution as the test function in derivation of local boundary integral equations, since both the displacements and tractions are unknown on the boundary of the interior sub-domain. Recent successes of the MLPG methods have been reported in the development of the MLPG finite-volume mixed method [Atluri, Han, and Rajendran (2004); Atluri et al. (2006a,b)], which was later extended to finite deformation analysis of static and dynamic problems [Han et al (2005)] and in simplified treatment of essential boundary conditions by a novel modified MLS procedure [Gao et al. (2006)]. The MLPG has been successfully applied for 2-D elastic problems in homogeneous and continuously nonhomogeneous solids [Sladek et al. (2004, 2005a, 2006); Sellountos et al. (2005); Ching and Chen (2006)]. The application of meshless methods to 3D problems has, hitherto, been very limited indeed. In this regard, Han et al. (2004a,b) have applied MLPG to elasticity in a homogeneous solid and the present authors have recently analyzed 3D heat conduction problems [Sladek et al. (2008)] and early also for axisymmetric boundary conditions [Sladek et al. (2005b, 2007)]. In this paper, the Heaviside step function is used as the test function. It yields a pure contour integral formulation on local boundaries for anisotropic elastostatics, while in elastodynamics an additional domain integral of inertia terms is involved. The spatial variation of the displacement is approximated by the moving least-square (MLS) scheme. After performing the spatial integrations, one obtains the system of ordinary differential equations for certain nodal unknowns. That system is solved numerically by the Houbolt finite difference scheme [Houbolt (1950)] as a time stepping method. Alternatively, the Laplace transform is applied to eliminate the time variable. Then, the local integral equations are derived for Laplace transforms. Several quasi-static boundary value problems have to be solved for various values of the Laplace transform parameter. The Papoulis inversion method

is applied to obtain the time-dependent solutions. The integral equations have a very simple nonsingular form. Moreover, both the contour and domain integrations can be easily carried out on spherical sub-domains. The boundary conditions on the global boundary are satisfied by collocation of the MLS-approximation expressions for the displacements at boundary nodal points. To demonstrate the accuracy of the present method more numerical examples with simple and more complex geometry are considered for static and dynamic cases.

2 Equilibrium equations

Let us consider a linear elastodynamic problem in an anisotropic domain Ω bounded by the boundary Γ . The equilibrium equation can be expressed as

$$\sigma_{ij,j}(\mathbf{x},t) - \rho \ddot{u}_i(\mathbf{x},t) = -X_i(\mathbf{x},t), \quad (1)$$

where $\sigma_{ij}(\mathbf{x},t)$ is the stress tensor, $X_i(\mathbf{x},t)$ is the body force vector, ρ is the mass density and $u_i(\mathbf{x},t)$ the displacement vector and the dots indicate the second time derivative. Comma denotes partial differentiation with respect to the spatial coordinates. An elastostatical problem can be considered formally as a special case of the elastodynamical one, with omitting the acceleration $\ddot{u}_i(\mathbf{x},t)$ in the equilibrium equation (1). Therefore, both cases are analyzed simultaneously.

In the case of elastic material, the relation between stress and strain are given by Hooke's law for an anisotropic body

$$\sigma_{ij}(\mathbf{x},t) = C_{ijkl} \varepsilon_{kl}(\mathbf{x},t) = C_{ijkl} u_{k,l}(\mathbf{x},t), \quad (2)$$

where C_{ijkl} is the material tensor which exhibits the symmetries

$$C_{ijkl} = C_{jikl} = C_{klij}.$$

The traction vector $t_i(\mathbf{x},t)$ is related to the displacement vector through Cauchy's formula $t_i = \sigma_{ij} n_j$, which leads to

$$t_i(\mathbf{x},t) = C_{ijkl} u_{k,l}(\mathbf{x},t) n_j(\mathbf{x}), \quad (3)$$

where n_j denotes a unit outward normal vector.

The constitutive equations are frequently written through the second order tensor of material constants [Lekhnitskii (1963)]. Then, one can write for an orthotropic

material

$$\begin{bmatrix} \sigma_{11} \\ \sigma_{22} \\ \sigma_{33} \\ \sigma_{23} \\ \sigma_{13} \\ \sigma_{12} \end{bmatrix} = \begin{bmatrix} c_{11} & c_{12} & c_{13} & 0 & 0 & 0 \\ c_{12} & c_{22} & c_{23} & 0 & 0 & 0 \\ c_{13} & c_{23} & c_{33} & 0 & 0 & 0 \\ 0 & 0 & 0 & c_{44} & 0 & 0 \\ 0 & 0 & 0 & 0 & c_{55} & 0 \\ 0 & 0 & 0 & 0 & 0 & c_{66} \end{bmatrix} \begin{bmatrix} \varepsilon_{11} \\ \varepsilon_{22} \\ \varepsilon_{33} \\ 2\varepsilon_{23} \\ 2\varepsilon_{13} \\ 2\varepsilon_{12} \end{bmatrix}. \quad (4)$$

The compliance coefficients β_{ij} are obtained by the inversion of matrix \mathbf{C} in equation (4). For orthotropic material they can be expressed through Young's moduli and Poisson's ratios

$$\begin{aligned} \beta_{11} &= 1/E_1, & \beta_{22} &= 1/E_2, & \beta_{33} &= 1/E_3 \\ \beta_{12} &= \beta_{21} = -\nu_{12}/E_1 = -\nu_{21}/E_2, & \beta_{13} &= \beta_{31} = -\nu_{13}/E_1 = -\nu_{31}/E_3 \\ \beta_{23} &= \beta_{32} = -\nu_{23}/E_2 = -\nu_{32}/E_3, & \beta_{44} &= 1/G_{23}, \\ \beta_{55} &= 1/G_{13}, & \beta_{66} &= 1/G_{12}, \end{aligned} \quad (5)$$

where E_k are the Young's moduli referring to the axes x_k , G_{12} is the shear modulus for the plane, ν_{ij} are Poisson's ratios.

The following boundary and initial conditions are assumed

$$u_i(\mathbf{x}, t) = \tilde{u}_i(\mathbf{x}, t) \text{ on } \Gamma_u$$

$$t_i(\mathbf{x}, t) = \tilde{t}_i(\mathbf{x}, t) \text{ on } \Gamma_t$$

$$u_i(\mathbf{x}, t)|_{t=0} = u_i(\mathbf{x}, 0) \text{ and } \dot{u}_i(\mathbf{x}, t)|_{t=0} = \dot{u}_i(\mathbf{x}, 0) \text{ in } \Omega,$$

where Γ_u is the part of the global boundary with prescribed displacement while on Γ_t the traction vector is prescribed.

3 Local boundary integral equations in Laplace transform domain

Applying the Laplace transformation to the governing equation (1), we have

$$\bar{\sigma}_{ij,j}(\mathbf{x}, s) - \rho s^2 \bar{u}_i(\mathbf{x}, s) = -\bar{F}_i(\mathbf{x}, s), \quad (6)$$

where

$$\bar{F}_i(\mathbf{x}, s) = \bar{X}_i(\mathbf{x}, s) + s u_i(\mathbf{x}, 0) + \dot{u}_i(\mathbf{x}, 0)$$

is the redefined body force in the Laplace transform domain with initial boundary condition for displacements $u_i(\mathbf{x}, 0)$ and velocities $\dot{u}_i(\mathbf{x}, 0)$.

The Laplace transform of function $f(\mathbf{x}, t)$ is defined as

$$L[f(x,t)] = \bar{f}(x,s) = \int_0^\infty f(x,t)e^{-st}d\tau,$$

where s is the Laplace transform parameter.

Instead of writing the global weak form for the above governing equation, the MLPG methods construct the weak form over local subdomains such as Ω_s , which is a small region taken for each node inside the global domain [Atluri and Shen (2002)]. The local subdomains overlap each other, and cover the whole global domain Ω . The local subdomains could be of any geometric shape and size. In the current paper, the local subdomains are taken to be of spherical shape.

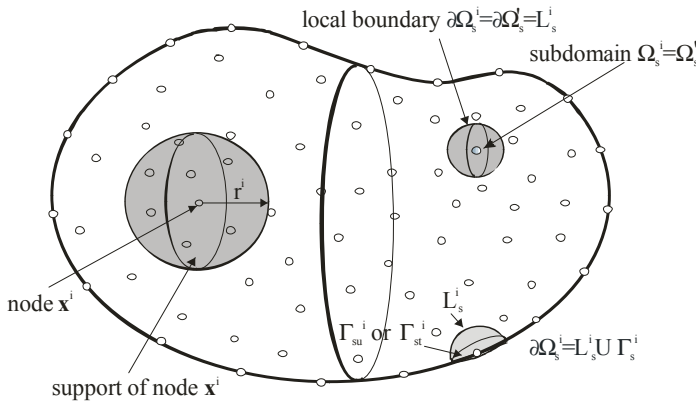


Figure 1: Local boundaries for weak formulation and support domain of weight function at node \mathbf{x}^i

The local weak form of the governing equation (6) can be written as

$$\int_{\Omega_s} [\bar{\sigma}_{ij,j}(\mathbf{x},s) - \rho s^2 \bar{u}_i(\mathbf{x},s) + \bar{F}_i(\mathbf{x},s)] u_{ik}^*(\mathbf{x}) d\Omega = 0, \tag{7}$$

where $u_{ik}^*(\mathbf{x})$ is a test function.

Using

$$\sigma_{ij,j} u_{ik}^* = (\sigma_{ij} u_{ik}^*)_{,j} - \sigma_{ij} u_{ik,j}^*$$

and applying the Gauss divergence theorem one can write

$$\int_{\partial\Omega_s} \bar{\sigma}_{ij}(\mathbf{x}, s) n_j(\mathbf{x}) u_{ik}^*(\mathbf{x}) d\Gamma - \int_{\Omega_s} \bar{\sigma}_{ij}(\mathbf{x}, s) u_{ik,j}^*(\mathbf{x}) d\Omega + \int_{\Omega_s} [-\rho s^2 \bar{u}_i(\mathbf{x}, s) + \bar{F}_i(\mathbf{x}, s)] u_{ik}^*(\mathbf{x}) d\Omega = 0, \quad (8)$$

where $\partial\Omega_s$ is the boundary of the local subdomain which consists of three parts $\partial\Omega_s = L_s \cup \Gamma_{st} \cup \Gamma_{su}$ (Fig.1). L_s is the local boundary that is totally inside global domain, Γ_{st} is the part of the local boundary which coincides with the global traction boundary, i.e., $\Gamma_{st} = \partial\Omega_s \cap \Gamma_t$, and similarly Γ_{su} is the part of local boundary that coincides with the global displacement boundary, i.e., $\Gamma_{su} = \partial\Omega_s \cap \Gamma_u$.

If a Heaviside step function is chosen as the test function $u_{ik}^*(\mathbf{x})$ in each subdomain

$$u_{ik}^*(\mathbf{x}) = \begin{cases} \delta_{ik} & \text{at } \mathbf{x} \in (\Omega_s \cup \partial\Omega_s) \\ 0 & \text{at } \mathbf{x} \notin \Omega_s \end{cases}$$

and considering

$$\bar{t}_i(\mathbf{x}, s) = \bar{\sigma}_{ij}(\mathbf{x}, s) n_j(\mathbf{x})$$

the local weak form (8) is leading to the local boundary integral equations

$$\int_{\partial\Omega_s} \bar{t}_i(\mathbf{x}, s) d\Gamma + \int_{\Omega_s} [-\rho s^2 \bar{u}_i(\mathbf{x}, s) + \bar{F}_i(\mathbf{x}, s)] d\Omega = 0. \quad (9)$$

Rearranging unknown terms on the left hand side we get

$$\int_{L_s} \bar{t}_i(\mathbf{x}, s) d\Gamma + \int_{\Gamma_{su}} \bar{t}_i(\mathbf{x}, s) d\Gamma - \int_{\Omega_s} \rho s^2 \bar{u}_i(\mathbf{x}, s) d\Omega = - \int_{\Gamma_{st}} \bar{t}_i(\mathbf{x}, s) d\Gamma - \int_{\Omega_s} \bar{F}_i(\mathbf{x}, s) d\Omega. \quad (10)$$

Equation (10) is recognized as the overall force equilibrium on the subdomain Ω_s . In case of stationary problems, the domain integral on the left hand side of this local boundary integral equation disappears. Then, a pure contour integral formulation is obtained under the assumption of vanishing body sources and homogeneous initial conditions.

In the MLPG method, the test and trial function are not necessarily from the same functional spaces. For internal nodes, the test function is chosen as the Heaviside

step function with support on the local subdomain. The trial function, on the other hand, is chosen to be the moving least squares (MLS) interpolation over a number of nodes randomly spread within the domain of influence. While the local subdomain is defined as the support of the test function on which the integration is carried out, the domain of influence is defined as a region where the weight function is not zero and all nodes lying inside are considered for interpolation. To approximate the distribution of the Laplace transform of displacements over a number of randomly located nodes $\{\mathbf{x}^a\}$, $a = 1, 2, \dots, n$, the MLS approximant $\bar{u}^h(\mathbf{x}, s)$ of \bar{u} , is defined by

$$\bar{u}^h(\mathbf{x}, s) = \mathbf{p}^T(\mathbf{x})\mathbf{a}(\mathbf{x}, s), \tag{11}$$

where $\mathbf{p}^T(\mathbf{x}) = [p^1(\mathbf{x}), p^2(\mathbf{x}), \dots, p^m(\mathbf{x})]$ is a complete monomial basis of order m ; and $\mathbf{a}(\mathbf{x})$ is a vector containing the coefficients $a^j(\mathbf{x})$, $j = 1, 2, \dots, m$ which are functions of the space co-ordinates $\mathbf{x} = [x_1, x_2, x_3]^T$. In 3D problems, the linear basis is defined as

$$\mathbf{p}^T(\mathbf{x}) = [1, x_1, x_2, x_3], \tag{12}$$

and the quadratic basis is defined as

$$\mathbf{p}^T(\mathbf{x}) = [1, x_1, x_2, x_3, (x_1)^2, (x_2)^2, (x_3)^2, x_1x_2, x_1x_3, x_3x_2]. \tag{13}$$

The coefficient vector $\mathbf{a}(\mathbf{x})$ is determined by minimizing a weighted discrete L_2 -norm defined as

$$J(\mathbf{x}) = \sum_{a=1}^n w^a(\mathbf{x}) [\mathbf{p}^T(\mathbf{x}^a)\mathbf{a}(\mathbf{x}, s) - \hat{\mathbf{u}}^a(s)]^2, \tag{14}$$

where $w^a(\mathbf{x})$ is the weight function associated with the node a with $w^a(\mathbf{x}) \geq 0$. Recall that n is the number of nodes in the support domain for which the weight function $w^a(\mathbf{x}) > 0$ and $\hat{\mathbf{u}}^a(s)$ are the fictitious nodal values, but not the nodal values of the unknown trial function $\bar{u}^h(\mathbf{x}, s)$, in general. The stationary condition of J in eq. (14) with respect to $\mathbf{a}(\mathbf{x}, s)$,

$$\partial J / \partial \mathbf{a} = 0,$$

leads to the following linear relation between $\mathbf{a}(\mathbf{x}, s)$ and $\hat{\mathbf{u}}(s)$

$$\mathbf{A}(\mathbf{x})\mathbf{a}(\mathbf{x}, s) - \mathbf{B}(\mathbf{x})\hat{\mathbf{u}}(s) = 0, \tag{15}$$

where

$$\mathbf{A}(\mathbf{x}) = \sum_{a=1}^n w^a(\mathbf{x})\mathbf{p}(\mathbf{x}^a)\mathbf{p}^T(\mathbf{x}^a),$$

$$\mathbf{B}(\mathbf{x}) = [w^1(\mathbf{x})\mathbf{p}(\mathbf{x}^1), w^2(\mathbf{x})\mathbf{p}(\mathbf{x}^2), \dots, w^n(\mathbf{x})\mathbf{p}(\mathbf{x}^n)]. \quad (16)$$

The MLS approximation is well defined only when the matrix \mathbf{A} in eq. (16) is non-singular. A necessary condition to satisfy this requirement is that at least m weight functions are non-zero (i.e. $n \geq m$) for each sample point $\mathbf{x} \in \Omega$. The solution of eq. (16) for $\mathbf{a}(\mathbf{x}, s)$ and a subsequent substitution into eq. (11) lead to the following relation

$$\bar{\mathbf{u}}^h(\mathbf{x}, s) = \mathbf{\Phi}^T(\mathbf{x}) \cdot \hat{\mathbf{u}}(s) = \sum_{a=1}^n \phi^a(\mathbf{x}) \hat{\mathbf{u}}^a(s), \quad (17)$$

where

$$\mathbf{\Phi}^T(\mathbf{x}) = \mathbf{p}^T(\mathbf{x})\mathbf{A}^{-1}(\mathbf{x})\mathbf{B}(\mathbf{x}). \quad (18)$$

In eq. (17), $\phi^a(\mathbf{x})$ is usually referred to as the shape function of the MLS approximation corresponding to the nodal point \mathbf{x}^a . From eqs. (16) and (18), it can be seen that $\phi^a(\mathbf{x}) = 0$ when $w^a(\mathbf{x}) = 0$. In practical applications, $w^a(\mathbf{x})$ is often chosen such that it is non-zero over the support of the nodal point \mathbf{x}_i . The support of the nodal point \mathbf{x}^a is usually taken to be a sphere of the radius r_i centred at \mathbf{x}^a (see Fig. 1). The radius r_i is an important parameter of the MLS approximation because it determines the range of the interaction (coupling) between the degrees of freedom defined at considered nodes.

A 4th-order spline-type weight function is applied in the present work

$$w^a(\mathbf{x}) = \begin{cases} 1 - 6\left(\frac{d^a}{r^a}\right)^2 + 8\left(\frac{d^a}{r^a}\right)^3 - 3\left(\frac{d^a}{r^a}\right)^4 & 0 \leq d^a \leq r^a \\ 0 & d^a \geq r^a \end{cases}, \quad (19)$$

where $d^a = \|\mathbf{x} - \mathbf{x}^a\|$ and r^a is the radius of the spherical support domain. With eq. (19), the C^1 -continuity of the weight function is ensured over the entire domain, therefore the continuity condition of the traction vector is satisfied.

The partial derivatives of the MLS shape functions are obtained as [Atluri (2004)]

$$\phi_{,k}^a = \sum_{j=1}^m \left[p_{,k}^j (\mathbf{A}^{-1}\mathbf{B})^{ja} + p^j (\mathbf{A}^{-1}\mathbf{B}_{,k} + \mathbf{A}_{,k}^{-1}\mathbf{B})^{ja} \right], \quad (20)$$

wherein $\mathbf{A}_{,k}^{-1} = (\mathbf{A}^{-1})_{,k}$ represents the derivative of the inverse of \mathbf{A} with respect to x_k , which is given by

$$\mathbf{A}_{,k}^{-1} = -\mathbf{A}^{-1}\mathbf{A}_{,k}\mathbf{A}^{-1}.$$

The traction vectors $\bar{t}_i(\mathbf{x}, s)$ at a boundary point $\mathbf{x} \in \partial\Omega_s$ are approximated in terms of the same nodal values $\hat{\mathbf{u}}^a(s)$ as

$$\bar{\mathbf{t}}^h(\mathbf{x}, s) = \mathbf{N}(\mathbf{x})\mathbf{C} \sum_{a=1}^n \mathbf{B}^a(\mathbf{x})\hat{\mathbf{u}}^a(s), \tag{21}$$

where the matrix $\mathbf{N}(\mathbf{x})$ is related to the normal vector $\mathbf{n}(\mathbf{x})$ on $\partial\Omega_s$ by

$$\mathbf{N}(\mathbf{x}) = \begin{bmatrix} n_1 & 0 & 0 & 0 & n_3 & n_2 \\ 0 & n_2 & 0 & n_3 & 0 & n_1 \\ 0 & 0 & n_3 & n_2 & n_1 & 0 \end{bmatrix}$$

and the matrix \mathbf{B}^a is represented by the gradients of the shape functions as

$$\mathbf{B}^a = \begin{bmatrix} \phi_{,1}^a & 0 & 0 \\ 0 & \phi_{,2}^a & 0 \\ 0 & 0 & \phi_{,3}^a \\ 0 & \phi_{,3}^a & \phi_{,2}^a \\ \phi_{,3}^a & 0 & \phi_{,1}^a \\ \phi_{,2}^a & \phi_{,1}^a & 0 \end{bmatrix}.$$

It should be noted that there are neither Lagrange multipliers nor penalty parameters introduced into the local weak form in eq. (7) because the essential boundary conditions on Γ_{su}^i can be imposed directly using the interpolation approximation eq. (17):

$$\sum_{a=1}^n \phi^a(\mathbf{x}^i)\hat{\mathbf{u}}^a(s) = \bar{\tilde{\mathbf{u}}}(\mathbf{x}^i, s) \text{ for } \mathbf{x}^i \in \Gamma_{su}^i, \tag{22}$$

where $\bar{\tilde{\mathbf{u}}}(\mathbf{x}^i, s)$ is the Laplace transform of displacements prescribed on the boundary Γ_{su}^i for essential boundary conditions.

Natural boundary conditions for the traction vector are satisfied on Γ_{st}^i by collocation of the approximate expression eq. (21) at \mathbf{x}^i

$$\mathbf{N}(\mathbf{x}^i)\mathbf{C} \sum_{a=1}^n \mathbf{B}^a(\mathbf{x}^i)\hat{\mathbf{u}}^a(s) = \bar{\tilde{\mathbf{t}}}(\mathbf{x}^i, s) \text{ for } \mathbf{x}^i \in \Gamma_{st}^i. \tag{23}$$

Furthermore, in view of the MLS-approximation (17) and (21) for unknown fields in the local integral equations (10), we obtain the discretized LIE

$$\sum_{a=1}^n \left(\int_{L_s^i} \mathbf{N}(\mathbf{x})\mathbf{C}\mathbf{B}^a(\mathbf{x})d\Gamma - \mathbf{I}\rho s^2 \int_{\Omega_s^i} \phi^a(\mathbf{x})d\Omega \right) \hat{\mathbf{u}}^a(s) = - \int_{\Omega_s^i} \bar{\tilde{\mathbf{F}}}(\mathbf{x}, s)d\Omega, \tag{24}$$

which are considered on the sub-domains adjacent to interior nodes \mathbf{x}^i . Note that \mathbf{I} stands in eq. (24) for the diagonal unit 3×3 matrix.

Collecting the discretized LIE together with the discretized boundary conditions, we get the complete system of algebraic equations for computation of nodal unknowns which are the Laplace transforms of fictitious parameters $\hat{\mathbf{u}}^a(s)$. The time dependent values of the transformed variables can be obtained by an inverse transformation. There are many inversion methods available for the Laplace transformation. As the Laplace transform inversion is an ill-posed problem, small truncation errors can be greatly magnified in the inversion process and lead to poor numerical results. In the present analysis the Papoulis algorithm [Papoulis (1957)] is used. This method has been used since it is less time consuming than other more advanced inversion techniques. An approximate value f_a of the inverse $f(t)$ for a specific time t is given by

$$f_a(t) = \sum_{i=1}^N C_i \sin(2i - 1)\Theta \quad (25)$$

where

$$\cos \Theta = e^{-bt}, \quad C_i = \sum_{k=1}^N B_{ik}^{-1} A_k$$

$$A_k = \frac{4}{\pi} 2^{2(k-1)} b \bar{f}[(2k-1)b], \quad k = 1, 2, \dots, N \quad (26)$$

And B_{ik}^{-1} is a triangular matrix whose elements are known and dependent on the number of the expansion coefficients N in eq. (25). The selected number $N = 15$ with a double precision arithmetic is applied in numerical examples. It means that it is needed to solve N boundary value problems for the corresponding Laplace parameters $s = (2k - 1)b$, where b is a real positive number. Its value determines the final time instant in which we want to obtain $f(t)$.

4 Time dependent Local integral equations

The local weak form of the governing equation (1) can be written as

$$\int_{\Omega_s} [\sigma_{i,j,j}(\mathbf{x}, t) - \rho \ddot{u}_i(\mathbf{x}, t) + X_i(\mathbf{x}, t)] u_{ik}^*(\mathbf{x}) d\Omega = 0. \quad (27)$$

Applying the Gauss divergence theorem to the first integral one obtains

$$\int_{\partial\Omega_s} \sigma_{ij}(\mathbf{x}, t) n_j(\mathbf{x}) u_{ik}^*(\mathbf{x}) d\Gamma - \int_{\Omega_s} \sigma_{ij}(\mathbf{x}, t) u_{ik,j}^*(\mathbf{x}) d\Omega + \int_{\Omega_s} [-\rho \ddot{u}_i(\mathbf{x}, t) + X_i(\mathbf{x}, t)] u_{ik}^*(\mathbf{x}) d\Omega = 0. \quad (28)$$

If we will use the same test function as in the Laplace transform approach, the local integral equation (LIE) has the form

$$\int_{L_s} t_i(\mathbf{x}, t) d\Gamma + \int_{\Gamma_{su}} t_i(\mathbf{x}, t) d\Gamma - \int_{\Omega_s} \rho \ddot{u}_i(\mathbf{x}, t) d\Omega = - \int_{\Gamma_{st}} \tilde{t}_i(\mathbf{x}, t) d\Gamma - \int_{\Omega_s} X_i(\mathbf{x}, t) d\Omega. \quad (29)$$

Substituting the MLS approximations for displacements (17) and tractions (27) into (29), we get the set of discretized LIEs

$$\sum_{a=1}^n \left[\left(\int_{L_s^i} \mathbf{N}(\mathbf{x}) \mathbf{C} \mathbf{B}^a(\mathbf{x}) d\Gamma \right) \hat{\mathbf{u}}^a(t) - \mathbf{I} \rho \left(\int_{\Omega_s^i} \phi^a(\mathbf{x}) d\Omega \right) \ddot{\mathbf{u}}^a(t) \right] = - \int_{\Omega_s^i} \mathbf{X}(\mathbf{x}, t) d\Omega, \quad (30)$$

considered at internal nodes \mathbf{x}^i . The discretized displacement and traction boundary conditions

$$\sum_{a=1}^n \phi^a(\mathbf{x}^i) \hat{\mathbf{u}}^a(t) = \tilde{\mathbf{u}}(\mathbf{x}^i, t) \text{ for } \mathbf{x}^i \in \Gamma_{su}^i, \quad (31)$$

$$\mathbf{N}(\mathbf{x}) \mathbf{C} \sum_{a=1}^n \mathbf{B}^a(\mathbf{x}^i) \hat{\mathbf{u}}^a(t) = \tilde{\mathbf{t}}(\mathbf{x}^i, t) \text{ for } \mathbf{x}^i \in \Gamma_{st}^i. \quad (32)$$

are considered at boundary nodes Γ_u and Γ_t , respectively.

The system of ordinary differential equations (30) and collocation equations (31) and (32) can be rearranged in such a way that all known quantities are on the r.h.s. Thus, in matrix form the system becomes

$$\mathbf{L} \ddot{\mathbf{x}} + \mathbf{K} \mathbf{x} = \mathbf{P}. \quad (33)$$

There are many time integration procedures for the solution of this system of ordinary differential equations. In the present work, the Houbolt method is applied. In

the Houbolt finite difference scheme [Houbolt (1950)], the acceleration ($\ddot{\mathbf{u}} = \ddot{\mathbf{x}}$) is expressed as

$$\ddot{\mathbf{x}}_{\tau+\Delta\tau} = \frac{2\mathbf{x}_{\tau+\Delta\tau} - 5\mathbf{x}_{\tau} + 4\mathbf{x}_{\tau-\Delta\tau} - \mathbf{x}_{\tau-2\Delta\tau}}{\Delta\tau^2}, \quad (34)$$

where $\Delta\tau$ is the time step.

Substituting eq. (34) into eq. (33), we get the system of algebraic equations for the unknowns $\mathbf{x}_{\tau+\Delta\tau}$:

$$\left[\frac{2}{\Delta\tau^2} \mathbf{L} + \mathbf{K} \right] \mathbf{x}_{\tau+\Delta\tau} = \mathbf{L} \frac{1}{\Delta\tau^2} \{ 5\mathbf{x}_{\tau} - 4\mathbf{x}_{\tau-\Delta\tau} + \mathbf{x}_{\tau-2\Delta\tau} \} + \mathbf{P}. \quad (35)$$

The value of the time step has to be appropriately selected with respect to material parameters (propagation velocities) and time dependence of the boundary conditions.

5 Numerical examples

5.1 A cube under uniform tension

In this section, numerical results will be presented to illustrate the implementation and effectiveness of the MLPG method for elasticity problems. First, homogeneous material properties and steady-state boundary conditions are considered. An anisotropic cube is analyzed.

In the first example, the cube is under a uniaxial tension in x_3 direction. Due to symmetry of boundary conditions with respect to 3 axes only one eighth of the cube is analyzed. Then, mixed boundary conditions for displacements and the traction vector on surfaces of the cube are considered (Fig. 2). For the purpose of illustration, a relatively coarse node distribution is shown in the figure.

In such a case, an analytical solution is available

$$u_1 = \beta_{13} \sigma_{33} x_1, \quad u_2 = \beta_{23} \sigma_{33} x_2, \quad u_3 = \beta_{33} \sigma_{33} x_3. \quad (36)$$

Numerical analyses are made for a cube with side $a = 10m$ and transversely isotropic and orthotropic material properties. For transversely isotropic material we have considered: Young's moduli $E_1 = 20 \cdot 10^4 kN/m^2$, $E_3 = 4 \cdot 10^4 kN/m^2$, Poisson's ratio $\nu_{12} = \nu_{13} = \nu_{23} = 0.25$ and shear moduli $G_{12} = 8 \cdot 10^4 kN/m^2$, $G_{13} = G_{23} =$

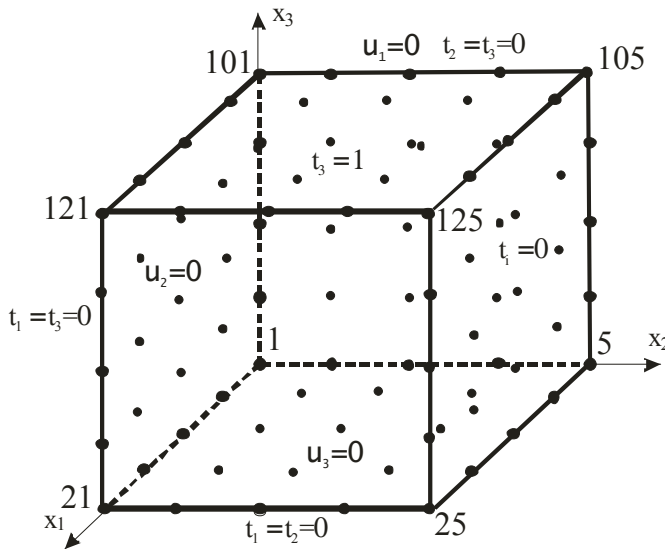


Figure 2: Mixed boundary conditions for analyzed cube

$1.6 \cdot 10^4 \text{ kN/m}^2$. Then, the corresponding stress-strain matrix is given as

$$\begin{bmatrix} 88 & 72 & 40 & 0 & 0 & 0 \\ & 88 & 40 & 0 & 0 & 0 \\ & & 24 & 0 & 0 & 0 \\ & & & 1.6 & 0 & 0 \\ \text{sym.} & & & & 1.6 & 0 \\ & & & & & 8 \end{bmatrix} \cdot 10^4 \text{ kN/m}^2.$$

The compliance coefficients β_{ij} can be obtained by inversion of the above matrix. For orthotropic material we have considered following material parameters: $E_1 = 20 \cdot 10^4 \text{ kN/m}^2$, $E_2 = 10 \cdot 10^4 \text{ kN/m}^2$, $E_3 = 4 \cdot 10^4 \text{ kN/m}^2$, $\nu_{12} = 0.5$, $\nu_{21} = 0.25$, $\nu_{23} = 0.25$, $\nu_{32} = 0.1$, $\nu_{13} = 0.25$, $\nu_{31} = 0.05$, $G_{12} = 8 \cdot 10^4 \text{ kN/m}^2$, $G_{13} = G_{23} = 1.6 \cdot 10^4 \text{ kN/m}^2$. Following identities have to be satisfied

$$E_2 \nu_{12} = E_1 \nu_{21}, \quad E_2 \nu_{32} = E_3 \nu_{23}, \quad E_3 \nu_{13} = E_1 \nu_{31}.$$

Constitutive equations for an orthotropic material are given as

$$\varepsilon_{11} = \frac{1}{E_1} \sigma_{11} - \frac{\nu_{21}}{E_2} \sigma_{22} - \frac{\nu_{31}}{E_3} \sigma_{33}$$

$$\begin{aligned}
\varepsilon_{22} &= -\frac{\nu_{12}}{E_1} \sigma_{11} + \frac{1}{E_2} \sigma_{22} - \frac{\nu_{32}}{E_3} \sigma_{33} \\
\varepsilon_{33} &= -\frac{\nu_{13}}{E_1} \sigma_{11} - \frac{\nu_{23}}{E_2} \sigma_{22} + \frac{1}{E_3} \sigma_{33} \\
2\varepsilon_{23} &= \frac{1}{G_{23}} \sigma_{23}, \quad 2\varepsilon_{13} = \frac{1}{G_{13}} \sigma_{13}, \quad 2\varepsilon_{12} = \frac{1}{G_{12}} \sigma_{12}.
\end{aligned} \tag{37}$$

The compliance matrix is computed from equations (37). After the inversion of the compliance matrix one gets the stress-strain matrix \mathbf{C}

$$\begin{bmatrix}
23.64 & 6.364 & 1.818 & 0 & 0 & 0 \\
& 11.97 & 1.515 & 0 & 0 & 0 \\
& & 4.242 & 0 & 0 & 0 \\
& & & 1.6 & 0 & 0 \\
& sym. & & & 1.6 & 0 \\
& & & & & 8
\end{bmatrix} \cdot 10^4 \text{ kN/m}^2.$$

In the MLS approximation, three regular node distributions with a total 27, 125 and 1331 nodes are used here. The radius of the spherical subdomain is considered as $r_{loc} = 0.8s$, where s is the shortest distance of two neighboring nodes. The numerical results can be compared with analytical ones. The Sobolev norms of the errors for the displacements obtained

$$r_u = \frac{\|u^{num} - u^{exact}\|}{\|u^{exact}\|} \times 100\% \text{ with } \|u\| = \left(\int_{\Omega} u_i u_i^d \Omega \right)^{1/2}$$

are 0.64%, 0.39% and 0.12% for particular node distributions with 27, 125 and 1331 nodes, respectively. One can see that a high accuracy of results is obtained even for a coarse node distribution.

Next, the cube with functionally graded material properties is analyzed. In the test example, we have considered only $c_{33}(x_3) = c_{330}(1 + x_3/a)$ is varying with Cartesian coordinates and other terms of the matrix \mathbf{C} are constant. Uniform material properties are the same as in the previous example for the orthotropic material.

The variation of displacements u_1 and u_2 along x_3 in the FGM cube edge ($x_1 = x_2 = 10$.) is presented in Fig. 3. One can see that both displacement components are gradually growing with x_3 in counterpart to a homogeneous cube where both components are uniform, $u_1^{hom} = -0.125 \cdot 10^{-7} m$ and $u_2^{hom} = -0.25 \cdot 10^{-7} m$. The present MLPG results are compared with ones obtained by the ANSYS computer code with 6400 solid186 elements. A very fine mesh is applied to use the FEM results as benchmark. One can observe a good agreement of results.

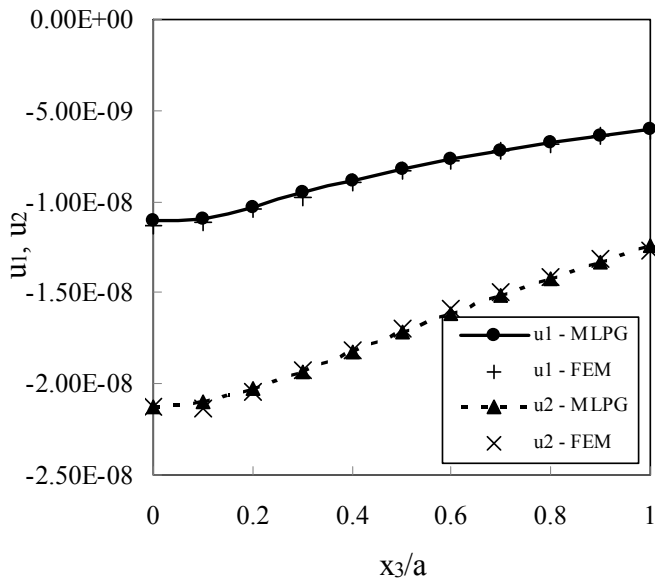


Figure 3: Variation of displacements u_1 and u_2 along x_3 in the FGM cube

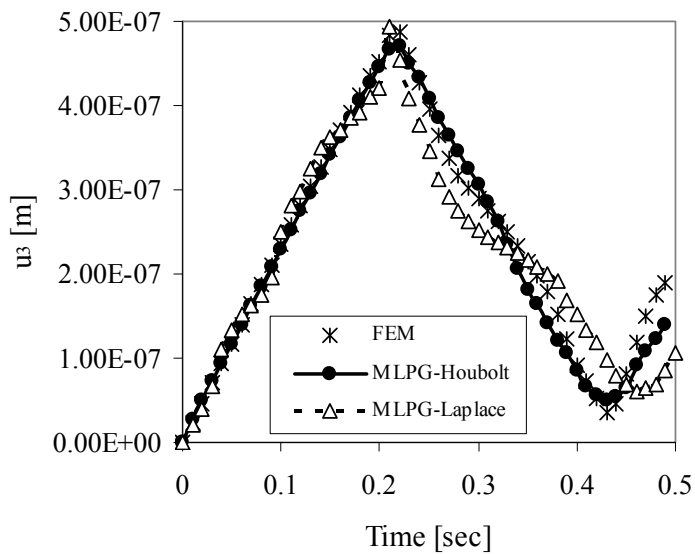


Figure 4: Temporal variation of displacements u_3 in the homogeneous cube at $x_1 = x_2 = x_3 = 10$.

Next, the same orthotropic cube with homogeneous material properties under an impact load with Heaviside time variation is analyzed. The mass density is considered as $\rho = 5000 \text{ kg/m}^3$. Both the Laplace transform and time difference approaches are applied to obtain numerical results. The Papoulis Laplace inversion is applied for 15 Laplace transform solutions and parameter $b = 1$. In the time difference approach we have used 100 time steps with time increment $t = 0.005s$. Numerical results for the vertical component of displacements at the top side of the cube are presented in Fig. 4. One can observe a very good agreement of FEM and MLPG results obtained by Houbolt time difference technique. A good agreement of the FEM and MLPG results obtained with Laplace transform method is observed only for shorter time instants. It is well known that the Laplace inversion techniques are unstable for large time instants.

The horizontal components of displacements are given in Fig. 5. Since Young's moduli are various in all three directions, we have three different wave velocities. Then, each displacement component has its own time variation. The displacement component u_1 oscillates around the static value $u_1^{stat} = -1.25 \cdot 10^{-8}$. Similarly, u_2 oscillates around the static value $u_2^{stat} = -2.5 \cdot 10^{-8}$.

Figure 6 presents a comparison of the time variations for u_3 at the top and mid side of the homogeneous orthotropic cube. On the top side where also external load is applied, one can observe immediate displacement increments. However, in the mid side it is observed certain delay due to a finite wave velocity.

Finally we have considered the cube with functionally graded material properties. Again, we have considered linear variation for $c_{33}(x_3) = c_{330}(1 + x_3/a)$ and other terms of the matrix \mathbf{C} are constant. Uniform material properties are the same as in the previous example for the orthotropic material. Numerical results are presented in Fig. 7. Very good agreement of the FEM and MLPG results with those by the time difference technique is observed on the top side of the cube. The peak values of u_3 for FGM cube are reduced with respect to the homogeneous case. Also peak value is reached at a shorter time instant in the FGM cube than in homogeneous one. It is due to higher wave velocity in FGM cube where mass density is considered as in the homogeneous case.

5.2 Hollow cylinder

An isotropic hollow cylinder subjected to a static pressure p_0 on the internal surface as shown in Fig. 8 is analyzed as a test example. Functionally graded hollow cylinder with a length $L = 0.3$ and radii $a = 4$ and $b = 5$ is investigated. The finite-length cylinder is considered as a part of the infinite-length tube. Hence, the axial displacements on the top and the bottom of the hollow cylinder are assumed to be vanishing. An exponential spatial variation of Young's modulus in radial direction

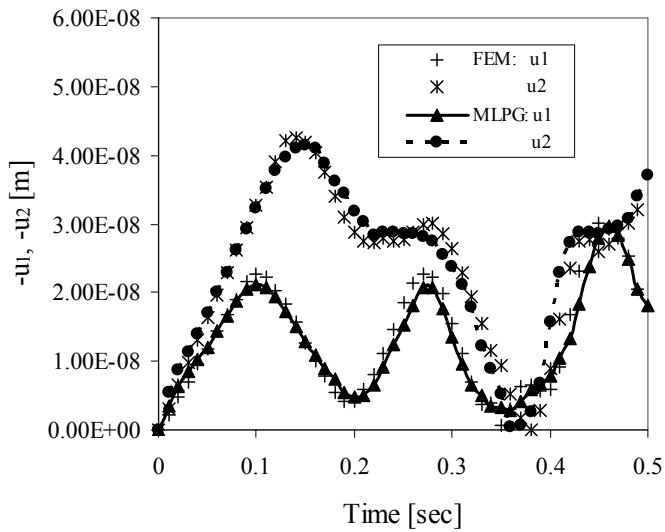


Figure 5: Temporal variation of displacements u_1 and u_2 in the homogeneous cube at $x_1 = x_2 = x_3 = 10$.

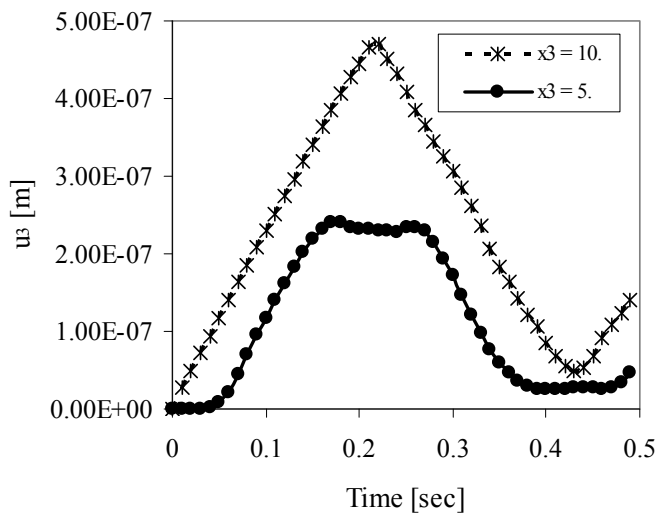


Figure 6: Temporal variation of displacements u_3 in the homogeneous cube at the top and mid side

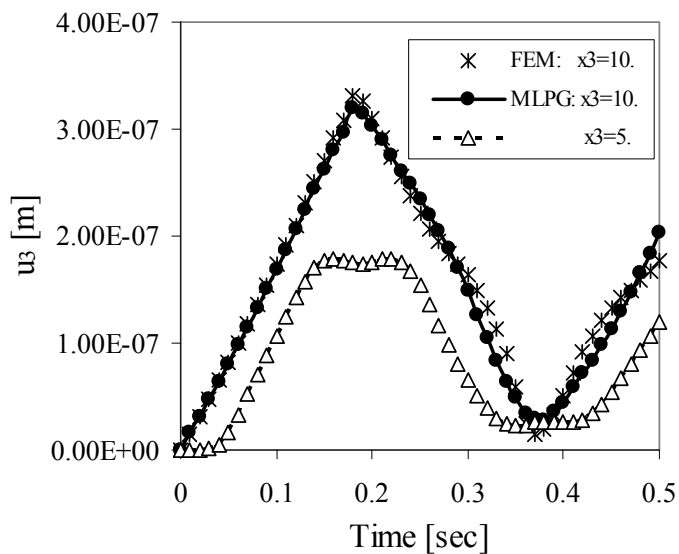


Figure 7: Temporal variation of displacements u_3 in the FGM cube at the top and mid side

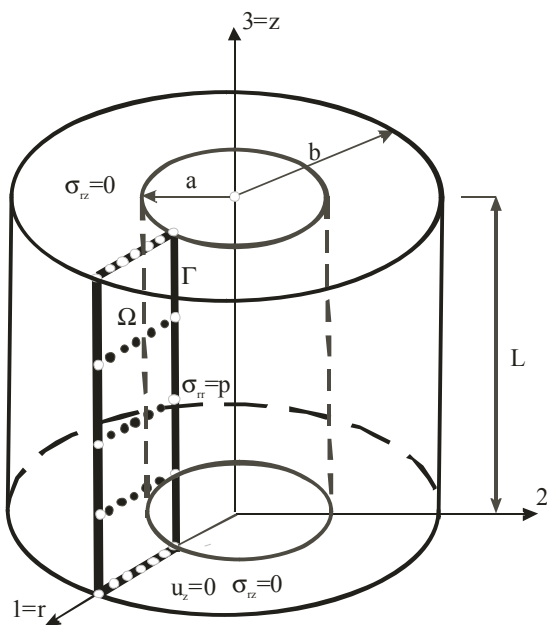


Figure 8: Geometry of a 3-d axisymmetric body

is considered:

$$E = E_1 \exp[\beta(r - a)], \tag{38}$$

where $\beta = \frac{1}{b-a} \ln(E_2/E_1)$ with $E_1 = E(a)$ and $E_2 = E(b)$.

Poisson’s ratio is taken as constant $\nu = 0.25$ and $E_1 = 10^4$. For a homogeneous hollow cylinder, $E(r) = E_1$ and $\beta = 0$. In this case, under the plane strain condition corresponding to an infinite-length tube, the analytical solution is available and it is given by

$$\begin{aligned} \sigma_{\varphi\varphi} &= \sigma_0 \left[(b/r)^2 + 1 \right], \quad \sigma_0 = \frac{p_0}{(b/a)^2 - 1}, \\ u_r &= \frac{\sigma_0}{E_1} r \left[(1 + \nu)(b/r)^2 + 1 - \nu \right]. \end{aligned} \tag{39}$$

In the error and convergence analyses, the following relative percentage errors of L_2 -norm are introduced for the radial displacement and the hoop stress as

$$e_u = \frac{\|u^{num} - u^{exact}\|}{\|u^{exact}\|}, \quad e_s = \frac{\|\sigma^{num} - \sigma^{exact}\|}{\|\sigma^{exact}\|}, \tag{40}$$

where

$$\|u\| = \left(\int_{\Omega} (u_r)^2 d\Omega \right)^{1/2}, \quad \|\sigma\| = \left(\int_{\Omega} (\sigma_{\varphi\varphi})^2 d\Omega \right)^{1/2}.$$

The relative percentage errors and the convergence rates for three different node distributions are presented in Fig. 9, where s represents the node-distance in radial direction. A uniform node distribution is considered in angular direction with nodes each 10 degrees. The accuracy is very high especially for the finest node distribution consisting of 3780 (21x5x36) nodes uniformly distributed in the rectangular domain with 21 nodes in the radial direction and 5 nodes in axial direction. In other two cases, 1584 (11x4x36) and 864 (6x4x36) nodes have been used.

Next, the influence of the gradation of the material properties on the radial displacements and the hoop stresses is analyzed. In Figs. 10 and 11 the following notation is used: $u_1 = u_r(a)$, $u_2 = u_r(b)$, $s_1 = \sigma_{\varphi\varphi}(a)$ and $s_2 = \sigma_{\varphi\varphi}(b)$. The numerical results provided by the MLPG method are compared with those obtained by the FEM-ANSYS computer code. Axisymmetric triangular elements with a quadratic interpolation have been used in the FEM analysis. In the FEM calculations, there have been used 100 elements in the radial direction and 10 elements in the axial

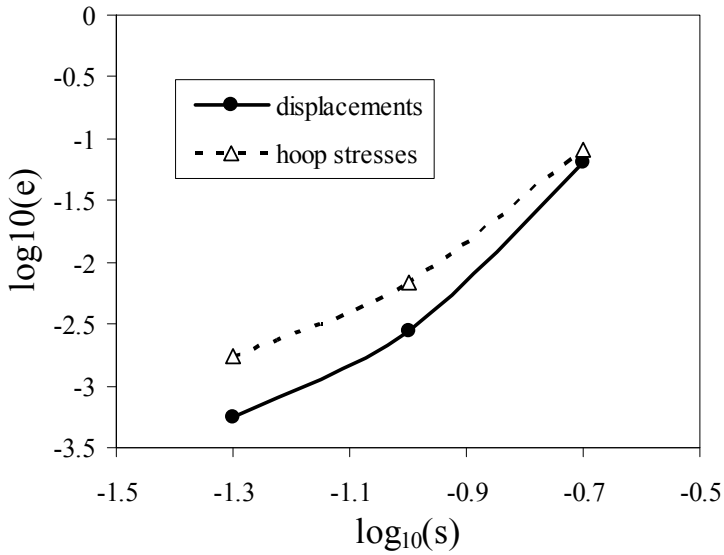


Figure 9: Relative errors and convergence rates

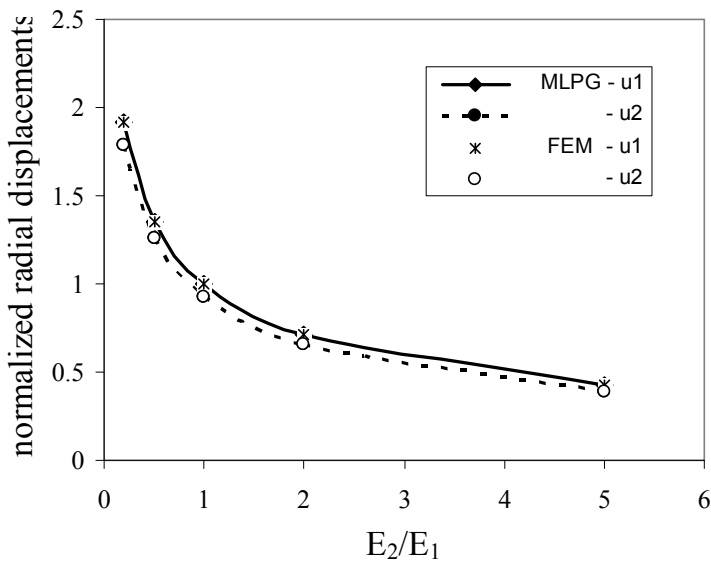


Figure 10: Variation of the normalized radial displacement with the nonhomogeneity ratio E_2/E_1

direction, with a total number of 1000 elements for the rectangular cross-section of the hollow cylinder with the axial plane. A good agreement between both results is achieved, which verifies the accuracy of the present meshless method. For convenience, the radial displacements are normalized by $u_r(a)$ and the hoop stresses by $\sigma_{\varphi\varphi}(a)$.

The hollow cylinder under an impact load $\sigma_{rr}(t) = pH(t - 0)$ on the internal surface of the hollow cylinder is analyzed too. The same material constants as in the previous static case are chosen. The mass density is taken as $\rho = 500$.

The time variations of the radial displacement on the internal surface of the hollow cylinder are shown in Figs. 12 and 13 for two different gradient parameters of Young's modulus. A node distribution consisting of 3780 (21x5x36) nodes uniformly distributed in the rectangular domain is used for our MLPG analysis. The Houbolt method has been applied for the MLPG with the time increment $t = 0.009s$. In the FEM analysis, the same mesh as in the previous static analysis is used now. The time step for FEM is selected as 0,002. A very good agreement between the FEM and the MLPG results is obtained. It verifies again the accuracy of the present method. In the FGM hollow cylinder with a gradually increasing Young's modulus in the radial direction characterized by $E_2/E_1 = 5.$, the frequency of the oscillations is higher as compared to that in a homogeneous hollow cylinder, but the amplitude is reduced. The opposite phenomena are observed in Fig. 13, where Young's modulus is gradually decreasing with radial coordinate.

Figure 14 presents the time variation of the hoop stresses on the internal surface of the hollow cylinder for the material gradations $E_2/E_1 = 5$. Numerical results for a homogeneous and an FGM hollow cylinder are given here to investigate the influence of the material gradation on the variation of the hoop stresses. If Young's modulus is gradually increasing with radial coordinate the hoop stress at the internal surface is significantly reduced in comparison with that in a homogeneous cylinder. It should be noted here that the same values of Young's modulus on the internal surface are used in both homogeneous and FGM hollow cylinders.

6 Conclusions

A meshless method based on the local Petrov-Galerkin approach is proposed for solution of static and elastodynamic problems in 3-D continuously non-homogeneous anisotropic bodies. For transient elastodynamic problems either the Laplace transform or the time difference techniques are applied.

The Heaviside step function is used as test functions in the local symmetric weak form, leading to the derivation of the local boundary-domain integral equations. In contrast to conventional boundary integral equation methods, all the integrands

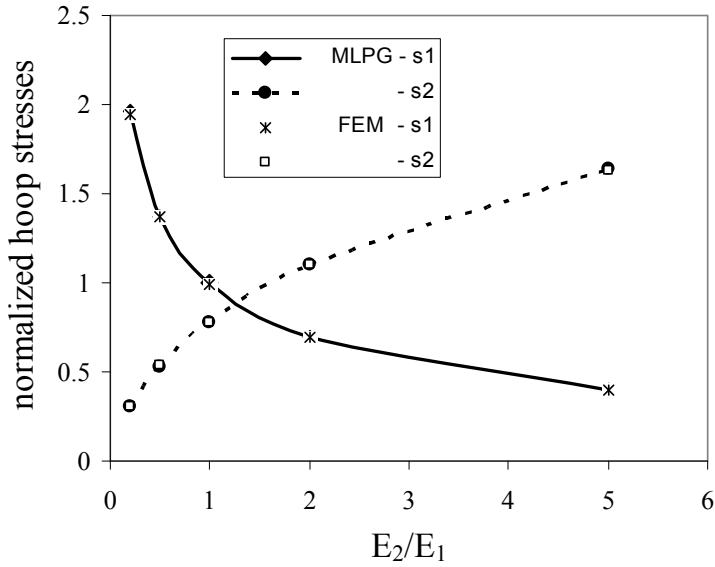


Figure 11: Variation of the normalized hoop stress with the nonhomogeneity ratio E_2/E_1

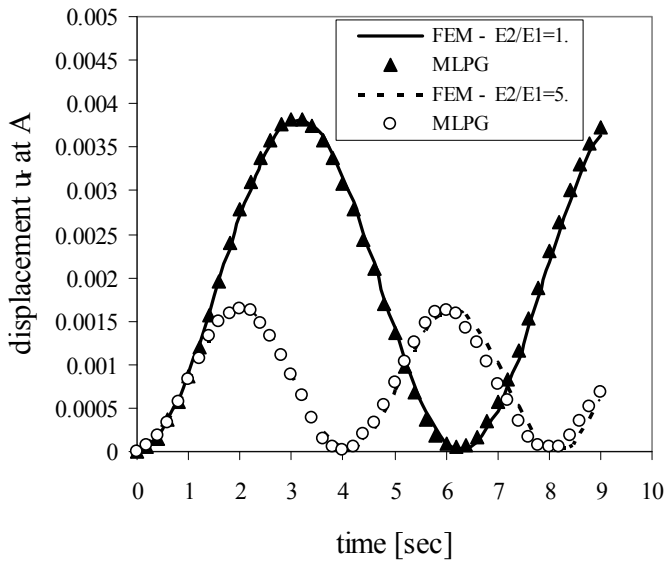


Figure 12: Time variation of the radial displacement on the internal surface of the FGM cylinder for $E_2/E_1 = 5$.

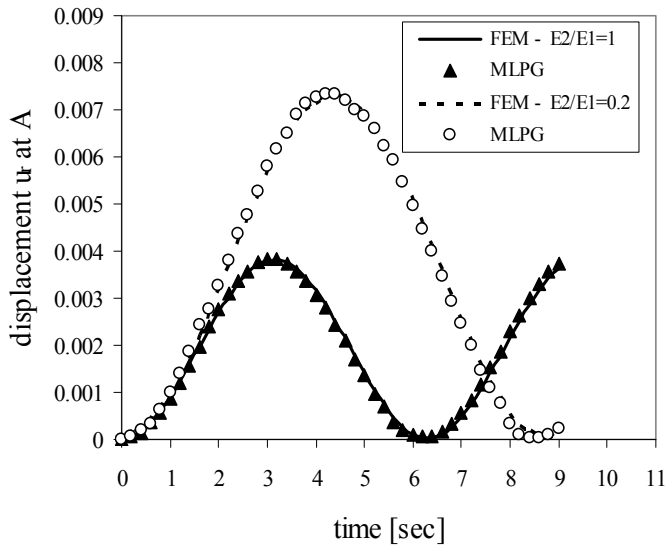


Figure 13: Time variation of the radial displacement on the internal surface of the FGM cylinder for $E_2/E_1 = 0.2$

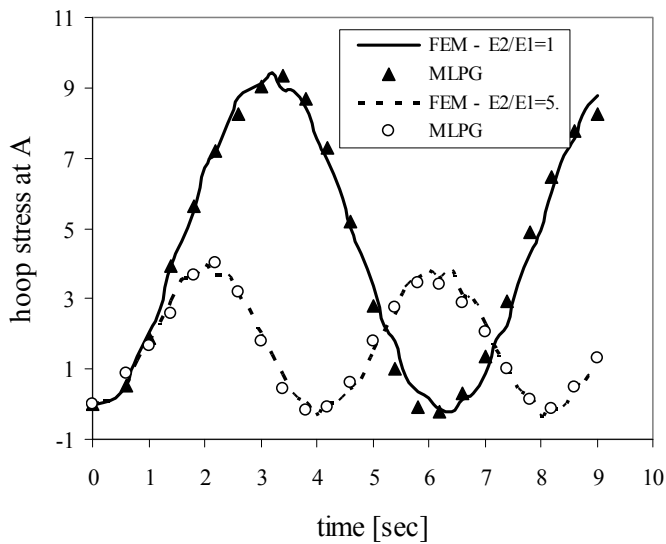


Figure 14: Time variation of the hoop stresses on the internal surface of the FGM cylinder for $E_2/E_1 = 5$.

in the present formulation are regular. Thus, no special integration techniques are required to evaluate the integrals.

The analyzed domain is divided into small overlapping spherical subdomains on which the local boundary integral equations are applied. The proposed methods are truly meshless methods, wherein no elements or background cells are involved in either the interpolation or the integration. The Moving Least-Squares (MLS) scheme is adopted for approximating the physical quantities.

The main advantage of the present method is its simplicity and generality in comparison to, say, the conventional BEM. The method is particularly promising for problems which cannot be solved by the conventional BEM when the fundamental solutions are not available. However, in its current development, the computational time in the proposed method is larger since there are many more nodes involved and the shape functions in the MLS approximation are significantly more complex than in BEM or FEM using simple polynomials. Intensive research to reduce the CPU is running. It is based on the reduction of the bandwidth of the final system matrix in the mixed formulation [Atluri et al. (2004), (2006b)].

The proposed method can be further extended to nonlinear problems, where meshless approximations may have certain advantages over the conventional domain-type discretization approaches.

Acknowledgement: The authors acknowledge the support by the Slovak Science and Technology Assistance Agency registered under number APVV-0427-07, the Slovak Grant Agency VEGA-2/0039/09.

References

Ang, W.T.; Telles, J. C.F. (2004): A numerical Green's function for multiple cracks in anisotropic bodies. *Journal of Engineering Mathematics*, 49: 197-207

Anlas, G.; Santare, M.H.; Lambros, J. (2000): Numerical calculation of stress intensity factors in functionally graded materials. *Int. J. Fracture*, 104: 131-143.

Atluri, S.N. (2004): *The Meshless Method(MLPG) for Domain & BIE Discretizations*, 688 pages, Tech Science Press, Forsyth, GA.

Atluri, S.N.; Zhu, T. (1998): A New Meshless Local Petrov-Galerkin (MLPG) Approach in Computational Mechanics, *Computational Mechanics*, 22: 117-127,

Atluri, S.N.; Sladek, J.; Sladek, V.; Zhu, T. (2000): The local boundary integral equation (LBIE) and its meshless implementation for linear elasticity. *Comput. Mech.*, 25: 180-198.

Atluri S.N.; Shen S. (2002): The Meshless Local Petrov-Galerkin (MLPG) Method:

A Simple & Less-costly Alternative to the Finite Element and Boundary Element Methods, *CMES: Computer Modeling in Engineering & Sciences*, 3: 11-52.

Atluri, S.N.; Han, Z.D.; Shen, S. (2003): Meshless local Petrov-Galerkin (MLPG) approaches for solving the weakly-singular traction & displacement boundary integral equations. *CMES: Computer Modeling in Engineering & Sciences*, 4: 507-516.

Atluri S.N.; Han Z.D.; Rajendran A.M. (2004): A new implementation of the meshless finite volume method, through the MLPG "Mixed" approach , *CMES: Computer Modeling in Engineering & Sciences*: 6: 491-513.

Atluri, S.N.; Liu, H.T.; Han, Z.D. (2006a): Meshless local Petrov-Galerkin (MLPG) mixed collocation method for elasticity problems. *CMES: Computer Modeling in Engineering & Sciences*, 14 (3): 141-152.

Atluri, S.N.; Liu, H.T.; Han, Z.D. (2006b): Meshless local Petrov-Galerkin (MLPG) mixed finite difference method for solid mechanics. *CMES: Computer Modeling in Engineering & Sciences*, 15 (1): 1-16.

Belytschko, T.; Krogauz, Y.; Organ, D.; Fleming, M.; Krysl, P. (1996): Meshless methods; an overview and recent developments. *Comp. Meth. Appl. Mech. Engr.*, 139: 3-47.

Brebbia, C.A.; Telles, J.C.F.; Wrobel, L.C. (1984): *Boundary Element Techniques*, Springer.

Chan, Y.; Gray, L.J.; Kaplan, T.; Paulino, G.H. (2004): Green's function for a two-dimensional exponentially graded elastic medium. *Proceedings Royal Society London A*, 460: 1689-1706.

Ching, H.K.; Chen, J.K. (2006): Thermomechanical analysis of functionally graded composites under laser heating by the MLPG method. *CMES: Computer Modeling in Engineering & Sciences*, 13 (3): 199-217.

Clements, D.L.; Haselgrove, M.D. (1983): A boundary integral equation method for a class of crack problems in anisotropic elasticity, *International Journal of Comput. Math.*, 12: 267-278.

Criado, R.; Ortiz, J.E.; Mantic, V.; Gray, L.J.; Paris, F. (2007): Boundary element analysis of three-dimensional exponentially graded isotropic elastic solids. *CMES: Computer Modeling in Engineering & Sciences*, 22 (2): 151-164.

Criado, R.; Ortiz, J.E.; Mantic, V.; Gray, L.J.; Paris, F. (2008): Green's function for three dimensional exponentially graded elasticity. *International Journal for Numerical Methods in Engineering*, 74: 1560-1591.

Cruse, T.A.; Swedlow, J.L. (1971): *Interactive Program for Analysis and Design Problems in Advanced Composites Technology*. Carnegie-Mellon University Re-

port AFML-TR-71-268.

Ding, H.; Liang, J.; Chen, B. (1997): The unit point force solution for both isotropic and transversely isotropic media. *Communications in Numerical Methods in Engineering*, 13: 95-102.

Dumir, P.C.; Mehta, A.K. (1987): Boundary element solution for elastostatic orthotropic half-plane problems. *Computer & Structures* 26: 431-438.

Eshelby, J.D.; Read, W.T.; Shockley, W. (1953): Anisotropic elasticity with applications to dislocations. *Acta Metallurgica*, 1: 251-259.

Gao, L.; Liu, K.; Liu, Y. (2006): applications of MLPG method in dynamic fracture problems. *CMES: Computer Modeling in Engineering & Sciences*, 12 (3): 181-195.

Han, Z.D.; Atluri, S.N. (2004a): Meshless local Petrov-Galerkin (MLPG) approaches for solving 3D problems in elasto-statics. *CMES: Computer Modeling in Engineering & Sciences*, 6: 169-188.

Han, Z.D.; Atluri, S.N. (2004b): A meshless local Petrov-Galerkin (MLPG) approach for 3-dimensional elasto-dynamics. *CMC: Computers, Materials & Continua*, 1: 129-140.

Han, Z.D.; Rajendran, A.N.; Atluri, S.N. (2005): Meshless Local Petrov-Galerkin (MLPG) approaches for solving nonlinear problems with large deformations and rotations. *CMES: Computer Modeling in Engineering & Sciences*, 10 (1): 1-12.

Houbolt, J.C. (1950): A recurrence matrix solution for the dynamic response of elastic aircraft. *Journal of Aeronautical Sciences*, 17: 371-376.

Kim J.H.; Paulino G.H. (2002) Isoparametric graded finite elements for nonhomogeneous isotropic and orthotropic materials. *J. Appl. Mech.* 69: 502-514.

Lekhnitskii, S.G. (1963): *Theory of Elasticity of an Anisotropic Body*, Holden Day.

Martin, P.A.; Richardson, J.D.; Gray, L.J.; Berger, J.R. (2002): On Green's function for a three-dimensional exponentially graded elastic solid. *Proceedings of Royal Society London A*, 458: 1931-1947.

Mikhailov, S.E. (2002): Localized boundary-domain integral formulations for problems with variable coefficients. *Engn. Analysis with Boundary Elements*, 26: 681-690.

Miyamoto, Y.; Kaysser, W.A.; Rabin, B.H.; Kawasaki, A.; Ford, R.G. (1999): *Functionally Graded Materials; Design, Processing and Applications*, Kluwer Academic Publishers, Dordrecht.

Pan, E.; Amadei, B. (1996): Fracture mechanics analysis of cracked 2-d anisotropic

media with a new formulation of the boundary element method. *International Journal of Fracture* 64: 161-174.

Pan, E.; Amadei, B.; Y.I. Kim (1998): 2-D BEM analysis of anisotropic half-plane problems – application to rock mechanics. *International Journal of Rock Mechanics and Mining Science & Beomechanics Abstracts*, 35: 195-218.

Pan, E. (1999): A BEM analysis of fracture mechanics in 2d anisotropic piezoelectric solids. *Engineering Analysis with Boundary Elements*, 23: 67-76.

Papoulis, A. (1957): A new method of inversion of the laplace transform. *Quarterly Applied Mathematics*, 14: 405-414.

Santare, M.H.; Lambros, J. (2000): Use of graded finite elements to model the behavior of nonhomogeneous materials, *Journal of Applied Mechanics* 67: 819-822.

Schlar, S.N. (1994): *Anisotropic Analysis Using Boundary Elements*, Computational Mechanics Publications.

Shiah, Y.C.; Tan, C.L.; Lee, V.G. (2008): Evaluation of explicit-form fundamental solutions for displacements and stresses in 3D anisotropic elastic solids. *CMES: Computer Modeling in Engineering & Sciences*, 34: 205-226.

Sladek, J.; Sladek, V.; Atluri, S.N. (2000): Local boundary integral equation (LBIE) method for solving problems of elasticity with nonhomogeneous material properties, *Computational Mechanics* 24: 456-462.

Sladek, J.; Sladek, V.; Atluri, S.N. (2001): A pure contour formulation for the meshless local boundary integral equation method in thermoelasticity. *CMES: Computer Modeling in Engineering & Sciences*, 2: 423-434.

Sladek, J.; Sladek, V.; Van Keer, R. (2003a): Meshless local boundary integral equation method for 2D elastodynamic problems. *Int. J. Num. Meth. Engn.*, 57: 235-249

Sladek, J.; Sladek, V.; Zhang, Ch. (2003b): Application of meshless local Petrov-Galerkin (MLPG) method to elastodynamic problems in continuously nonhomogeneous solids, *CMES: Computer Modeling in Engineering & Sciences*, 4: 637-648.

Sladek, J.; Sladek, V.; Atluri, SN. (2004) Meshless local Petrov-Galerkin method in anisotropic elasticity. *CMES: Computer Modeling in Engineering & Sciences* 6: 477-489.

Sladek, J.; Sladek, V.; Zhang, Ch. (2005a): Stress analysis in anisotropic functionally graded materials by the MLPG method, *Engn. Analysis with Boundary Elements*, 29: 597-609.

Sladek, J.; Sladek, V.; Krivacek, J.; Zhang, Ch. (2005b): Meshless Local Petrov-Galerkin Method for stress and crack analysis in 3-D axisymmetric FGM

bodies, *CMES: Computer Modeling in Engineering & Sciences* 8: 259-270.

Sladek, J.; Sladek, V.; Zhang, Ch.; Schanz, M. (2006): Meshless Local Petrov-Galerkin Method for Continuously Nonhomogeneous Linear Viscoelastic Solids. *Computational Mechanics*, 38: 279-289.

Sladek, J.; Sladek, V.; Hellmich, Ch.; Eberhardsteiner, J. (2007): Heat conduction analysis of 3D axisymmetric and anisotropic FGM bodies by meshless local Petrov-Galerkin method, *Computational Mechanics* 39: 323-333.

Sladek, J.; Sladek, V.; Tan, C.L.; Atluri, S.N. (2008): Analysis of transient heat conduction in 3D anisotropic functionally graded solids by the MLPG, *CMES: Computer Modeling in Engineering & Sciences* , 32 : 161-174.

Sellountos, E.J.; Vavourakis, V.; Polyzos, D. (2005): A new singular/hypersingular MLPG (LBIE) method for 2D elastostatics, *CMES: Computer Modeling in Engineering & Sciences*, 7: 35-48.

Snyder, M.D.; Cruse, T.A. (1975): Boundary integral analysis of anisotropic cracked plates. *International Journal of Fracture* 31: 315-328.

Sollero, P.; Aliabadi M.H. (1993): Fracture mechanics analysis of anisotropic plates by the boundary element method. *International Journal of Fracture* 64: 269-284.

Suresh, S.; Mortensen A. (1998): *Fundamentals of Functionally Graded Materials*. Institute of Materials, London.

Zhu, T.; Zhang, J.D.; Atluri, S.N. (1998): A local boundary integral equation (LBIE) method in computational mechanics, and a meshless discretization approach. *Comput. Mech.* 21: 223-235.

